Ion Implantation Enhanced Exfoliation Efficiency of V2AlC Single Crystals: Implications for Large V2CTz Nanosheet Production

Hanna Pazniak, Simon Hurand, Nadia Guignard, Stéphane Célérier, Ulf Wiedwald, Thierry Ouisse, Marie-Laure David, Vincent Mauchamp

Ion Implantation Enhanced Exfoliation Efficiency of V_2AlC Single Crystal: Implications for Large V_2CT_z Nanosheets Production

Hanna Pazniak,[*,†,‡] *Simon Hurand,*[†] *Nadia Guignard,*[&] *Stéphane Celerier,*[&] *Ulf Wiedwald,*[/] *Thierry Ouisse,*[‡] *Marie-Laure David,*[*,†] *Vincent Mauchamp*[*,†]

[†]Institute Pprime, UPR 3346 CNRS, Université de Poitiers, ISAE-ENSMA, BP 30179, 86962 Futuroscope-Chasseneuil Cedex, France

[‡‡] Université Grenoble Alpes, CNRS, Grenoble INP, LMGP, Grenoble, CS 50257, 38016 Grenoble Cedex 1, France

[&]Institut de Chimie des Milieux et Matériaux de Poitiers (IC2MP), Université de Poitiers, CNRS, F-86073 Poitiers, France

[/] Faculty of Physics and Center for Nanointegration (CENIDE), University of Duisburg-Essen, 47057 Duisburg, Germany

KEYWORDS: V_2AlC single crystal, ion-implantation, chemical etching, macroscopic V_2CT_z MXene, TEM-EELS

ABSTRACT. MXenes are two-dimensional transition metal carbides and nitrides with an attractive combination of physicochemical properties, gaining a notable potential in many

applications. Currently MXene synthesis is mainly performed from powder precursors which purity and grain size defines the quality and flake size of 2D sheets, typically not exceeding 2-3 μm. In this work, we successfully synthesized macroscopic nanolayered V_2CT_z MXenes with lateral dimensions larger than 25 μm from V_2AlC single crystal by exploiting a new strategy based on ion implantation. Ne^{2+} ion-implantation of the single crystal precursor is applied to introduce defects in the crystal structure of V_2AlC which facilitates chemical etching and drastically reduces the etching time down to 8 hours (~ 10 times lower as compared to conventional synthesis from powder precursors). The quality and morphology of exfoliated macroscopic MXene multilayers have been comprehensively studied by performing detailed analysis based on different kinds of microscopies and spectroscopies. The obtained macroscopic flakes are ideal objects to study the intrinsic physical properties of V_2CT_z MXenes and explore their potential application, in particular as membranes.

INTRODUCTION

MAX phases are nanolayered ternary and quaternary transition metal carbides and nitrides with the chemical formula of $M_{n+1}AX_n$ (n = 1, 2, 3), where M denotes to early transition metal, A is an A-group element and X represents C or N. [1] This class of materials crystallizes in the hexagonal structure and uniquely combines metal and ceramic properties. In this respect, MAX phases are easily machinable, relatively soft, electrically and thermally conductive, and excellent in their mechanical characteristics and chemical stability.[2] To date up to 155 compounds have been experimentally synthesized[2] and tested for many possible applications, in particular microelectronics, protective coatings in high-temperature and harsh radiation environments.[3] Recently MAX phases gained a further boost as precursors of a large class of two-dimensional

(2D) materials called MXenes with general formula of $M_{n+1}X_nT_z$ (T_z represents surface functional groups, predominantly =O, –OH, –F and –Cl)[4]. As opposed to most 2D materials, produced by easily breaking of weak out-of-plane van der Waals bonds in the corresponding bulk structures,[5] MXene precursors have quite strong metallic bonds between atomic layers[6] and require harsh conditions for conversion into 2D state. In particular, the use of concentrated fluorine-based environment, long etching time (up to 120 h) and temperature (up to 80 °C) defines the degree of removal of the A-element and the efficiency of the synthesis.[4] Recently, several alternative techniques have been developed to produce MXenes in particular using molten salts[7] or surface acoustic waves.[8] The use of molten salts prevents the oxidation of MXenes and, more importantly, provides unique halogen functionalization. While the use of surface acoustic waves drastically enhances the productivity.

As a result of chemical etching, the surface of MXenes is naturally functionalized and therefore demonstrates excellent processability by forming organic and inorganic based suspension,[9] polymer-based composites,[10] and viscous inks.[11] Apart from this, MXenes show optical transparency, tuneable electronic properties, and hereby already demonstrated their superiority with respect to other 2D materials in terms of metallic conductivity (11 000 S/cm)[12] and elastic characteristics (386±13 GPa).[13] However, the MXene research is mainly focused on application related studies[14-16] while the understanding of their fundamental physical properties is still in early stages and mainly related to theoretical investigations.[17,18]

A problem that hinders the experimental verification of the theoretical predicted properties of MXenes is related to the fact that the commonly measured systems are stacked 2D nanosheets or thin films, which due to the presence of various interfacial/interlayer phenomena hide their intrinsic characteristics. Therefore, single flakes are considered as ideal objects for the exploration

of the basic physical properties of MXenes. However, the production of individual flakes is quite critical due to the use of aforementioned harsh etching conditions, which causes many defects on the surface of the synthesized MXenes.[19] Even so recently proposed mild synthesis conditions[20,21] remarkably improve the quality of several MXene compositions, their flake size is non-uniform, relatively small (usually 2-3 μm; the maximum size of 10 μm is reported only for $Ti_3C_2T_z$ MXenes) and difficult to control. This is quite critical since flake size profoundly impacts the measured properties. For instance, $Ti_3C_2T_z$ MXenes with small lateral size (200-500 nm) are not suitable for the electrical measurements due to the low environmental stability.[22] On the opposite, large $Ti_3C_2T_z$ flakes (with the lateral size of 10 μm) demonstrates a huge value of conductivity up to 11,000 S/cm and field-effect electron mobilities up to 6 $cm^2/V \cdot s$.[10]

V_2CT_z is another interesting MXene structure produced by wet chemical etching in HF or mixture of HF and HCl.[20] Transparent V_2CT_z thin films produced by spin casting have a high figure of merit for optoelectronic properties, demonstrating their high potential in this field.[23] V_2CT_z freestanding film produced by vacuum-assisted filtration shows a high value of electrical conductivity (1000 S/cm).[20] The latter is attributed to the improved chemical stability of delaminated flakes and an increase in their lateral size (up to 2-3 μm).[20] The maximum lateral size and quality of MXene nanosheets are defined by the grain size, purity and stoichiometry of its MAX phase precursor.[24] In this respect, MAX phase single crystals can be considered as an ideal model system to synthesize macroscopic MXene flakes and to explore their properties. So far, there are only three studies reporting on chemical exfoliation of MXenes from MAX phase single crystal precursors, in particular V_2AlC[25,26] and V_4AlC_3.[27] In the case of V_2AlC, initially scratched single crystal[25] or crystal with designed pillars (from 7 μm to 500 μm lateral size)[26] are undergoing etching that take from 40 h[26] to 72 h.[25] In both cases the etching of V_2AlC single crystal is clearly

accelerated by the presence of defects and stresses, localized close to the crystal edges, resulting in a maximum exfoliated region of 100 μm.[25,26] While when a defect-free crystal is exposed to the chemical etching, the maximum penetration depth is reduced down to 25 μm.[26] In the case of V_4AlC_3 single crystal, the exfoliation for 40 days results in producing of submillimeter flakes.[27] Thus, the presence of defects vastly impacts the exfoliation process.

Considering the beneficial role of defects in facilitating chemical etching, and the results of our previous studies showing the selective damage in Al layers induced by ion implantation in Ti_3AlC_2 thin films,[28] we employ Ne^{+2} ion implantation of V_2AlC single crystal to introduce defects into the crystal structure. We demonstrate a complete chemical etching of Al layers from V_2AlC single crystal within the ion implanted region resulting in production of V_2CT_z MXene multilayers with a lateral size exceeding 25 μm. We found that defects induced by ion implantation in V-Al layers significantly reduces the etching time by 10 times down to 8 h. The detailed structural analysis (X-Ray diffraction, scanning electron microscopy, transmission electron microscopy) and spectroscopic characterization (electron energy-loss spectroscopy) confirms the production of large scale crystalline V_2CT_z MXenes. Macroscopic V_2CT_z will allow performing an in-depth study of its fundamental physical properties. In addition, the large size of multi-layered structure exfoliated from a single crystal would be extremely beneficial for its potential use as capacitor[29] and membrane.[30] In the latter case, the well-aligned layers resulting from the anisotropic structure of the single crystals can serve as transport channels, providing a better transfer of molecules than films consisting of staked small sheets. Moreover, the vastly enhanced synthesis will greatly accelerate the application of V_2CT_z MXenes, which already demonstrated their potential as optical transparent coatings,[23] photothermal agent[31] and in energy conversion.[32]

RESULTS AND DISCUSSION

Phase and microstructural characterization of ion-implanted V_2AlC single crystal before and after chemical etching

V_2AlC single crystals with typical dimensions of 0.5-2 cm were directly exposed to the ion beam as detailed in the Experimental Section and in **Figure 1a**. We applied the "Stopping and Range of Ions in Matter" (SRIM) software to simulate Ne^{2+} implantation induced damages in V_2AlC crystal structure (2.7×10^{12} ion/cm^2 fluence, 380 keV energy). **Figure 1b** shows the simulated damage profile which is asymmetric in shape and about 700 nm in depth. Based on the SRIM calculations, the implantation damage within the depth profile gradually increases from 0.04 dpa close to the surface up to a maximum value of 0.15 dpa at 480 nm depth and sharply decreases afterwards. According to Raman spectroscopy (*Figure S1, Supporting Information*), Ne^{2+}implantation at a fluence of 2.7×10^{12} ions/cm^2 (corresponding to 0.1 dpa) does not cause structural modification of V_2AlC as all Raman modes of the virgin crystal are detected on the implanted one. While an increase in fluence (corresponding to 0.2 dpa) leads to the disappearance of E_{2g} (158 cm^{-1}) and E_{1g} (240 cm^{-1}) with a slight shift of E_{2g} (258 cm^{-1}) and A_{1g} (365 cm^{-1}) modes due to structural modifications induced by implantation. This is in complete agreement with results showing a gradual structural modification without amorphization in V_2AlC for 1 MeV Au^+ irradiations corresponding to 0.15 to 0.2 dpa.[33] Since the most critical step in MXene etching is intercalation of the etchant between M-A layers, we can assume that Ne^{2+} implantation can induce some distortions in V-Al bonding, facilitating easier intercalation of etchant ions and reducing the processing time. This assumption is very consistent with the preferential alteration of the Al planes observed in Ti_3AlC_2 thin films irradiated with 240 keV Ar^+ ions.[33]

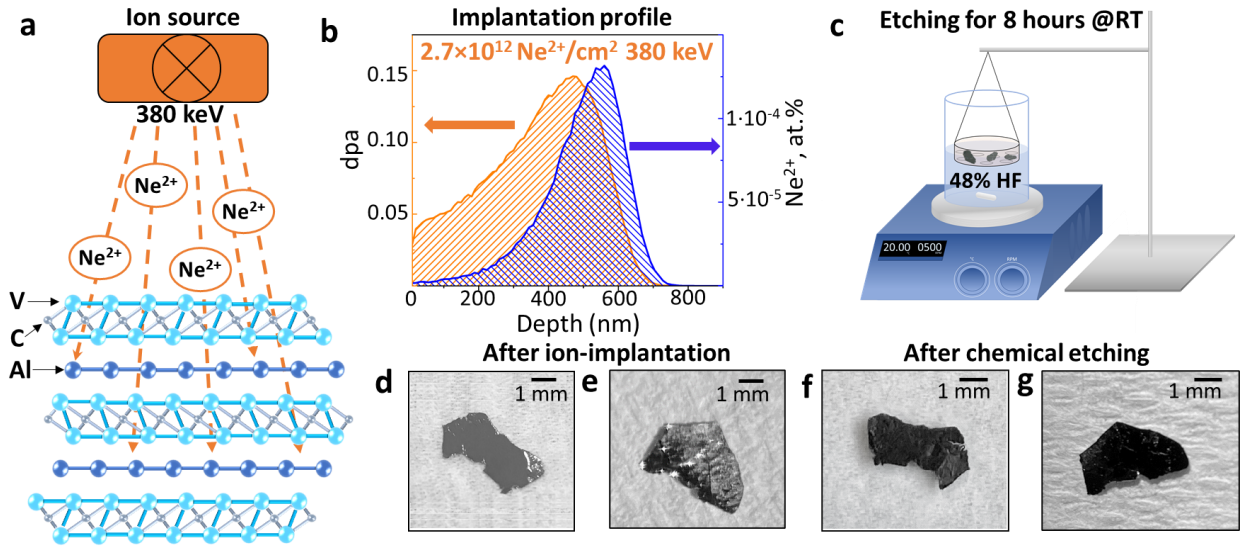

Figure 1. Schematic illustration of the fabrication process of V_2CT_z MXenes using ion implantation approach. **a** The implantation process of V_2AlC single crystal using a Ne^{2+} ions at 380 keV energy; **b** SRIM simulated damage (orange) and ion distribution profile (blue) within V_2AlC following the ion implantation Ne^{2+} ions with 2.7 × 10^{12} ion/cm^2 fluence; **c** Schematic representation of chemical etching of V_2AlC single crystals in 48% HF; Photographs of ion-implanted V_2AlC single crystals before **d, e** and after **f, g** chemical etching.

After the ion implantation, single crystals were immersed in the concentrated HF solution as described in detail in the Experimental Section and in **Figure 1c**. The surface of the single crystals before and after chemical etching is shown in Figure 1d, e and 1f, g respectively. During chemical etching the initially shiny grey metallic surface of single crystals (Figure 1d, e) is gradually changed towards black. After 8 h of chemical etching the implanted surface of single crystal is completely black (Figure 1f, g), while the opposite un-implanted surface remains grey. The appearance of black powder on the implanted surface of single crystal is the first indicator of the successful conversion of MAX phase to MXenes. *Ab initio* molecular dynamics simulation of the

etching process of Ti_3AlC_2 in HF solution[34] suggests that exfoliation of Ti_3C_2 MXene proceeds via HF insertion through edges of MAX phase. After the breaking of M-A bonds, the interlayer gap opens and thereby facilitates further insertion of HF molecules in the structure. The same mechanism was experimentally observed during HF etching of V_2AlC single crystal.[26] The observations were proven by the preferential loss of the Al species at the edges of the crystal as compared to the center with the maximum etched region of 100 µm. Interestingly, in our work the exfoliated region of V_2CT_z MXenes is largely extended up to mm's area. This finding highlights the crucial role of ion implantation in promoting chemical etching of single crystal. One possible reason is that the dissociated HF molecules react more easily with damaged Al planes and thereby enhance the penetration of F ions into the single crystal from the edges to the center. Moreover, the main benefit for the use of ion implantation manifests in the drastically reduced etching time, down to 8 h, as compared with conventionally used HF etching protocols of V_2AlC powder precursor (92 h),[31] recently reported milder etching conditions (72 h)[20] or equivalent single crystals (72 h).[25] To further elucidate the phase composition and microstructure of exfoliated single crystal, we performed detailed structural and morphological investigation presented in Figure 2.

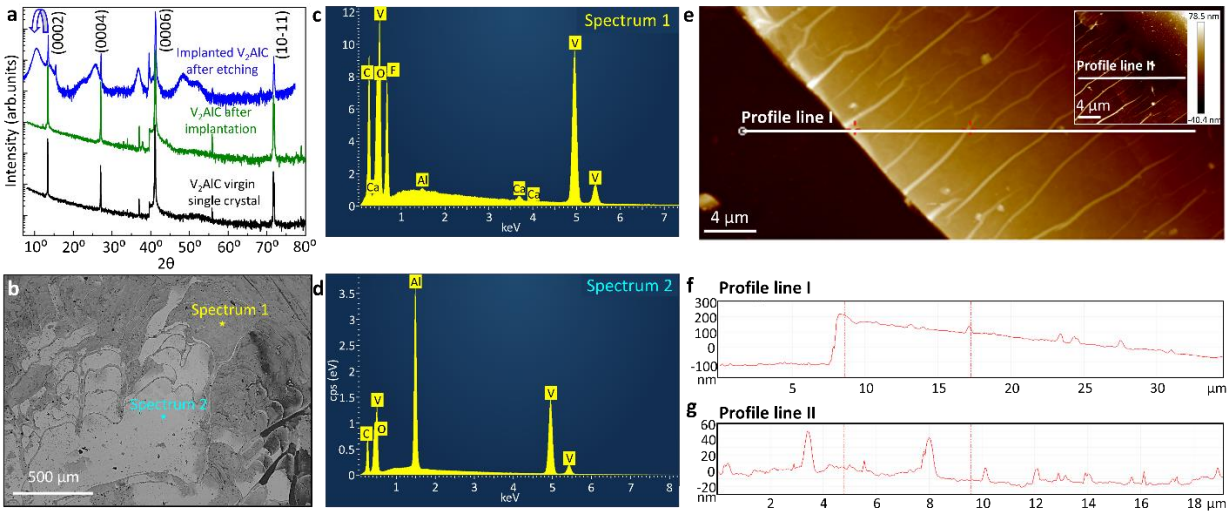

Figure 2. Structural and morphological characterization of V_2AlC single crystal before and after chemical etching. **a** XRD of virgin V_2AlC single crystal before (black curve), after ion implantation (green curve) and after etching (blue curve). **b** SEM image (BSE mode) of the ion implanted V_2AlC single crystal surface showing two regions: etched (dark grey, **Spectrum 1**) and the surface after scrapping part of the exfoliated layer (light grey, **Spectrum 2**). **c, d** EDS spectra of corresponding regions marked in **b**. **e, f** and **g** AFM image and corresponding height profiles of etched V_2AlC single crystal. **f** Height profile measured along the Profile line I in **e**. **g** Wrinkle height profile measured along the Profile line II given in the inset of figure **e**.

The XRD analysis of V_2AlC single crystals shows no changes in the phase composition induced by ion implantation (Figure 2a). In both cases (virgin and ion-implanted crystals), the XRD patterns display peaks originating from (000*l*) planes of V_2AlC, and the presence of a single (10-11) peak. After chemical etching, the sharp (000*l*) peaks are still present in the XRD pattern, indicating the preservation of V_2AlC MAX phase structure below the exfoliated surface. Additionally, characteristic high intensity broad peaks downshifted with respect to the MAX phase peaks are clearly seen in the XRD pattern of the V_2AlC after chemical etching. This confirms the successful removal of Al layers from V_2AlC structure within the implanted depth resulting in expansion of the interlayer distance and thus the increase of c-parameter from 13.1 Å to 17.5 Å. Further, we studied chemical composition of the surface of the single crystal after chemical exfoliation (black powder) by recording EDX spectra (Figure 2c). We observed the presence of V and C originated from V-C blocks in MAX phase structure and O and F elements appear after replacement of the etched Al layers, while a tiny signal corresponding to Al has been detected over a large area (*Table S1, Figure S2 Supporting Information*), showing that only a negligible amount of Al remains. This confirms, in addition to the XRD findings, that Al was successfully etched

from the ion implanted region of the single crystal. Afterwards, we scrapped part of the exfoliated layer until the grey single crystal surface was bare and recorded EDX spectra on this region (Figure 2d). We detected the signals of V, Al, and C elements, the stoichiometry of which is close to 2:1:1 corresponding to V_2AlC MAX phase (*Table S1, Supporting Information*). This finding further supports the assumption that the chemical conversion of MAX phase to 2D MXene is successful within the damaged region, which is about 700 nm based on SRIM calculation (**Figure 1b**). We used Monte Carlo simulation of electron trajectory in solids (CASINO v3) while performing EDX analysis, predicting a typical depth of 1 to 2 μm, probed for a V_2CT_z multilayer at 10 keV energy.

Figure 2 e,f,g presents an AFM image and corresponding height profiles of exfoliated V_2CT_z multilayer. The investigated part of V_2CT_z multilayer is quite large with a dimension of at least 20×30 μm, which is much larger as compared to a typical size of V_2CT_z produced from the powder precursor (usually less than 3 μm).[20] The analyzed region clearly reveals the presence of characteristic wrinkles along the exfoliated surface, a characteristic height profile of which is given in Figure 2g. The presence of such wrinkles is commonly found in large flakes of CVD grown graphene.[35] The length of wrinkles is quite large varying from 4 to 20 μm, which additionally confirms the production of large exfoliated V_2CT_z structures, at least of the same lateral size as wrinkles. The measured multilayer thicknesses are between 200 and 300 nm.

TEM and spectroscopic investigation of V_2CT_z MXenes

Transmission electron microscopy (TEM) and energy-filtered selected area electron diffraction (SAED) were initially used to perform structural investigations of V_2CT_z MXenes exfoliated from the single crystal. For TEM study, the fragments of black powder were detached by moving the grid over the exfoliated surface of the crystal and subjected to plane-view imaging. We studied

fragments of different sizes and thicknesses named as Zone 1 – Zone 3, the structural characterization is presented in Figure 3.

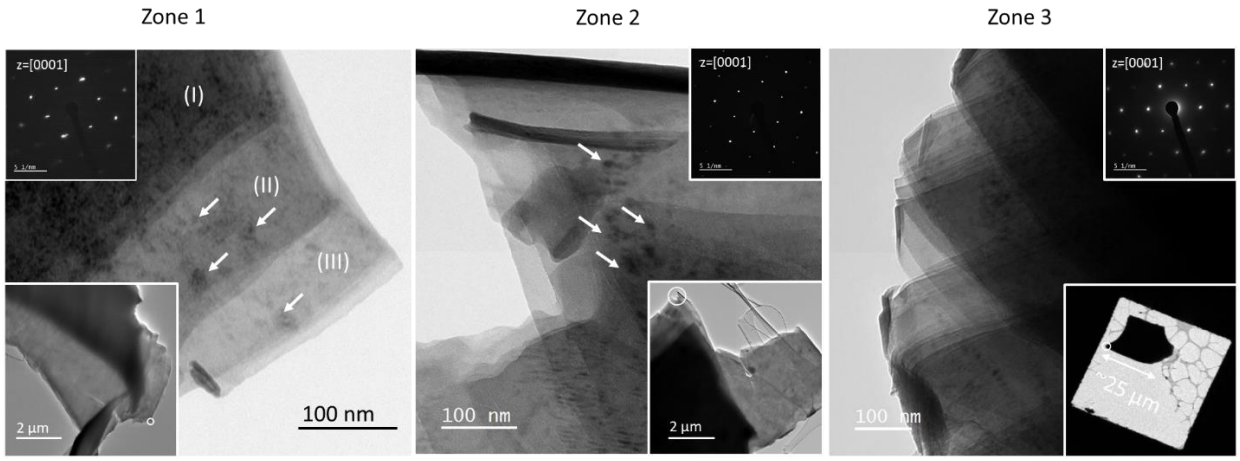

Figure 3. Structural characterization of V_2CT_z MXenes multilayers. TEM images of the studied fragments of the V_2CT_z MXenes exfoliated from corresponding V_2AlC single crystal (Zone 1 – Zone 3). The insets are overviews of the analysed region at lower magnification and corresponding SAED patterns of the enlarged area (SAED patterns were collected close to the [0001] zone axis). Areas where the main TEM images and corresponding EEL spectra were recorded are identified by white circles.

We observed that all investigated fragments are much larger (the lateral size varies from few µm (Zone 1, 2) to 25 µm (Zone 3)) as compared with the typical size of MXenes exfoliated from powder precursor (1-3 µm).[20-26,32] One can notice that the size of the largest fragment (*i.e.* Zone 3) is very consistent with that determined from the AFM measurements given in Figure 2e. By focusing on the edges of the exfoliated multilayered fragments we observe the presence of flake-like contrast with clearly visible thin delaminated regions. The fragments are flat comprising of different numbers of layers distinguished by contrast variation increasing from the edges to the

center (Zone 1). In addition, there is a pronounced TEM contrast with dark spots on the thin region of the multilayers (Zone 1 and Zone 2), which is a characteristic feature of radiation-induced damages.[36-38] The insets of Figure 3 show typical SAED patterns of exfoliated thin flakes. We observed that all regions have the characteristic for MXenes hexagonal-like structure originated from the single crystal precursor. The spots in the SAED patterns recorded on the flakes of Zones 2 and 3 are discrete and sharp, while the ones of Zone 1 are diffuse. This suggests a slight distortion of the crystal structure of V_2CT_z multilayers of Zone 1 caused by Ne^{2+} ion-implantation. We note the absence of any extra spots in the recorded SAED patterns, suggesting their environmental stability. As was previously reported[19,22], the large flakes are more oxidation resistant as compared with the flakes of smaller size. Moreover, due to the short etching time of 8 h, V_2CT_z flakes appear without visible etching induced through-flake holes that also contribute to flakes instability. Based on the SAED patterns we calculate the corresponding inter-reticular distances which are 0.26±0.01 nm for d_{100} and 0.15±0.01 nm for d_{110}. These values are consistent with that of reference V_2AlC.[39] To further study the chemical composition of the exfoliated MXene multilayers we focused on the fragment of the largest area of 25x10μm² (Zone 3) and performed EDX analysis at different positions within the flake, marked with differently colored dots as indicated in Figure 4.

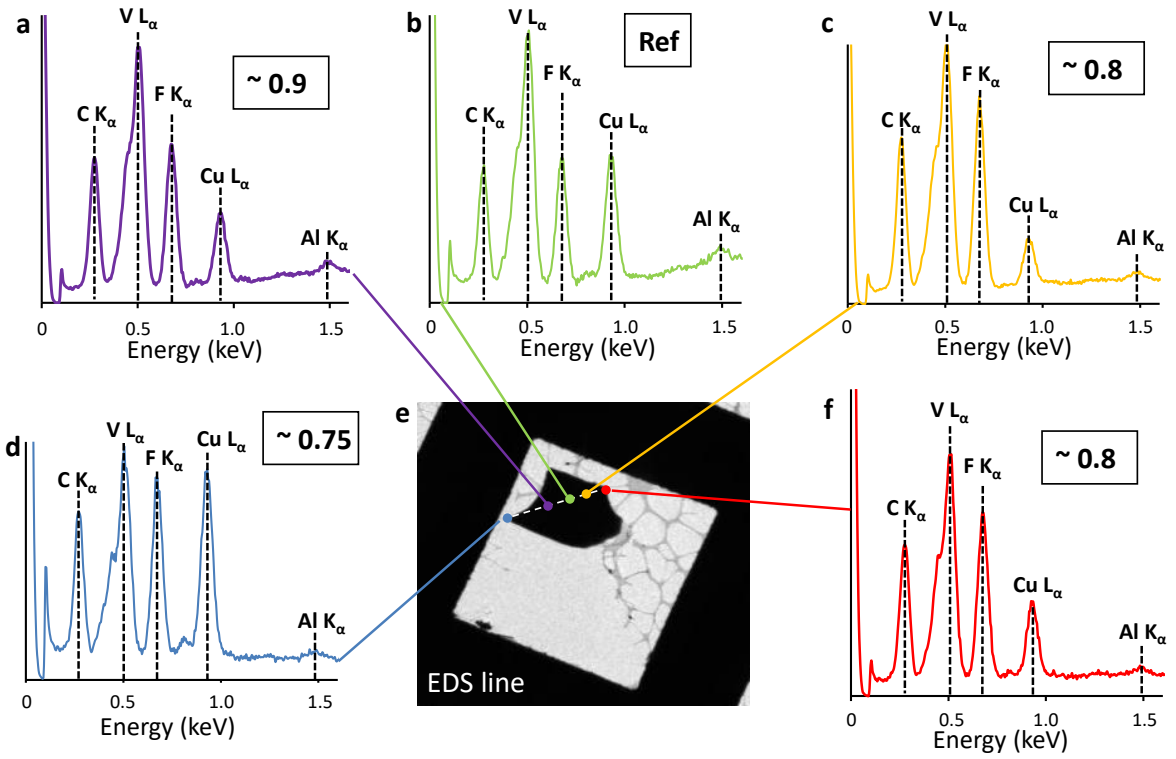

Figure 4. Chemical composition of the exfoliated V_2CT_z MXene multilayers. **e** TEM image of the V_2CT_z fragment (Zone 3) in the section of the TEM grid; **a, b, c, d, f** EDX spectra at different positions of the exfoliated fragment.

We detected the presence of V and C originated from the core MXene structure, Al remained from MAX phase structure and F attributed to the surface functional groups. The Cu signal comes from the TEM grid. There is almost no Al signal in the EDX spectra recorded at all positions of the studied fragment proving the complete chemical etching within the large crystal area. In addition to point EDS analysis, we performed elemental mapping of the exfoliated fragments with an approximate lateral size of 7 μm (Figure S3, Supporting Information). We observed a uniform distribution of the V, C, and F in the multilayer with a tiny amount of Al (0.3 at.%). This is in line with the conclusion of SEM-EDX results suggesting the successful chemical exfoliation of V_2AlC single crystal. We note that the relative intensities between the V-L_α, C-K_α and F-K_α vary

depending on the position in the fragment. This could be due to the compositional inhomogeneity within the exfoliated area. To estimate it, we normalized the EDX spectra to the V-L_α signal and compared the V/C ratios obtained along the line taking the third spectrum (*i.e.* the green one) as a reference; the corresponding values are given in the EDX plots. We find out that V/C ratio is probably smaller at the edges of the exfoliated regions as compared with the center part of the studied multilayer. This possibly could be due to the overetching process at the crystal edges, resulting in partial removal of V in addition to Al.

To further explore the elemental composition of the synthesized V_2CT_z MXenes and identify the chemical environment at the nanoscale, we performed electron energy-loss spectroscopy (EELS) of exfoliated multilayers. Figure 5 displays the characteristic core-loss and low-loss spectra recorded on different zones of the exfoliated crystal marked in Figure 3.

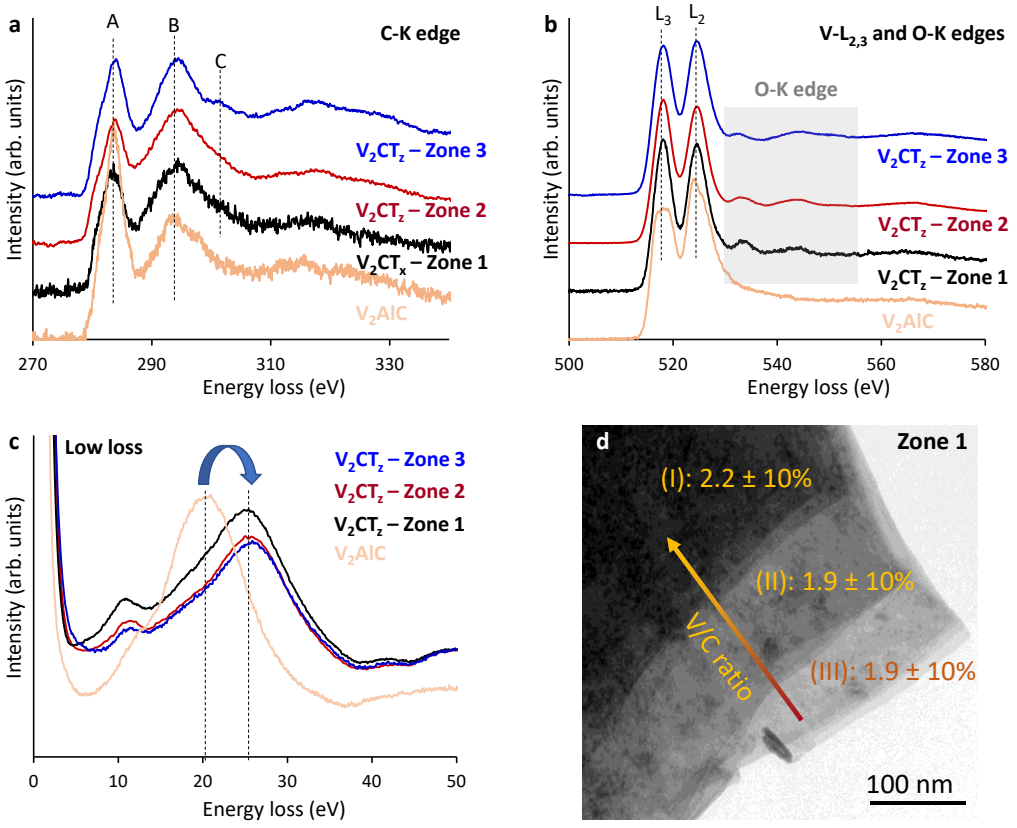

Figure 5. EEL spectra of exfoliated V_2CT_z multilayers. **a** C-K and **b** V-$L_{2,3}$ and O-K edges (grey area) and **c** low-loss spectra of exfoliated V_2CT_z fragments recorded on the different zones presented in figure 3. Spectra collected on V_2AlC powders are also given for comparison. Spectra are vertically shifted for clarity and lines are guide to the eyes. In **a**, spectra were aligned on the position of the first peak A and in **b** they were aligned on the position of the L_3 peak. **d** TEM image of the fragment of the V_2CT_z MXenes of Zone 1 with marked regions subjected to EELS quantification and calculated V/C ratio.

The characteristic C-K edges around 283.5 eV are reproducible for different zones. The C-K edge possesses well-resolved fine structure with the characteristic features previously reported for MXenes, in particular for $Ti_3C_2T_z$ and Ti_2CT_z.[40] Interestingly, in Zones 1 and 2, the peak located at 295 eV (labelled B) is quite broad as compared to that in Zone 3 where the shoulder labelled C can clearly be identified. As was theoretically and experimentally established in our previous works, the C-K edge is quite sensitive to the structural disorder resulting in a broadening of the fine structure at higher energy (*i.e.*, peaks B and C in the present case), the first peak A being mainly affected by surface disorder in Ti-based MXenes.[40,41] We thus suggest that the exfoliated multilayers are more damaged due to the implantation in Zones 1 and 2 than in Zone 3. That the structural disorder induced by implantation is not homogeneously distributed in different zones along the implantation profile is consistent with the damage profile given in Figure 1b and shows that there is room for reduction of radiation-induced damages in the MXene multilayers by adjusting the implantation conditions or by selecting only MXene flakes close to the surface of the crystal. Finally, comparison between the C-K edge in the MXene and in the corresponding MAX phase precursor clearly show a significant modification in the electronic structure after exfoliation with a strong decrease of the intensity of peak A; this is expected from the replacement of the Al

layers by terminal groups. This modification is confirmed at the V-$L_{2,3}$ edge (Figure 5b) which also evidence major changes between the MXene and V_2AlC with a strong change in the L_2/L_3 ratio characteristic of a modification in the V-3*d* bands.

The characteristic V-$L_{2,3}$ edges at 518 eV are also reproducible for different zones and exhibit well-defined fine structure with sharp peaks. By recording EEL spectra at the V-$L_{2,3}$ edges we clearly observe the presence of the O-K edge at 532 eV. This is attributed to the terminal groups on the surface of the exfoliated layers confirming successful etching. The F-K edge (see *Figure S4, Supporting Information*) was also clearly identified, further confirming the replacement of the Al layers in the MAX phase by the usually observed terminal groups of MXenes.

The experimental low-loss EEL spectra recorded on exfoliated fragments of the different zones are compared to the low-loss EEL spectra recorded on the V_2AlC MAX phase powders (Figure 5c). It should be noted that the main differences between the aforementioned spectra is the position of the bulk plasmon peak. This peak appears at around 20 eV in the V_2AlC MAX phase structure, while it is about 5 eV higher in the structure of exfoliated V_2CT_z multilayers. This shift is the characteristic feature of the exfoliation as demonstrated by Magné *et al.* in $Ti_3C_2T_x$,[42] and a strong proof of the successful conversion of MAX phases to MXenes. In addition, we performed the quantification of elements by EELS on the fragments of Zone 1 and calculated the V/C ratio correspondingly (Figure 5d). We choose three regions: at the edges of the exfoliated flakes (Zone III), in the centre (Zone I), and between them (Zone II). The precise elemental quantification by EELS is difficult due to the fact that O-K edge is superimposed to the V-$L_{2,3}$ edge. However, the calculated V/C ratio is close to the value in the initial MAX phase with 10% uncertainty. We observed that the quantification results are heterogeneous and depends on the region although the V/C ratio increases from the edge to the center (orange arrow, Figure 5d). This finding is consistent

with a possible V overetching on the edges of the single crystal as we already observed by EDX analysis and previously reported by Kim *et al.*[26]

CONCLUSION

This work demonstrates a new approach to produce macroscopic V_2CT_z multilayer MXenes from V_2AlC single crystal precursor by exploiting an ion-implantation strategy. It is based on the selective damaging of the Al layers with Ne^{2+} ion-implantation which drastically facilitate chemical etching of Al layers within the implanted region and reduce the exfoliation time by a factor of ~10 as compared to V_2AlC powder exfoliation or previously reported V_2AlC single crystal exfoliation. The complete conversion of implanted MAX phases to MXenes and formation of macroscopic 2D V_2CT_z flakes was comprehensively proven by XRD, SEM, EDX and TEM measurements. The lateral size of exfoliated fragments is much larger as compared with MXenes produced from powder precursors. By combining TEM and EELS results we found that the exfoliated nanosheets are quite stable with a slight distortion in the structure induced by ion-implantation. The macroscopic size of exfoliated flakes suggests they could be ideal objects to explore the fundamental physical properties of MXenes. In addition, the large size of the exfoliated V_2CT_z MXenes has potential in membrane applications due to the well-aligned layers resulting from the anisotropic structure of the single crystal precursor. Finally, we assume that using ion-implantation, an industrial compatible technique, could open new perspectives in MXene synthesis by largely enhancing the efficiency of the chemical etching of MAX phases.

EXPERIMENTAL SECTION

Growth and ion-implantation of V_2AlC single crystal. The V_2AlC single crystal precursors are grown *via* a flux growth method.[39] Growth takes place in alumina crucibles by using melted

pellets of vanadium and aluminum. The C incorporation is controlled by dipping a predetermined height of a rotating graphite rod in the solution at the maximum temperature for 2 h. After the high-temperature step, aimed at dissolving all elements, the temperature is slowly decreased (over days) to enhance Ostwald ripening and decrease the number of small crystals in the solution. Crystals are extracted from the flux by hydrochloric acid etching. The high-temperature solution growth parameters and the choice of the appropriate liquid composition as well as structural characterization of crystals are thoroughly described in Ref.39. To perform ion-implantation, V_2AlC single crystals are mounted on a sample holder having an implantation surface of about 10 cm^2 and directly exposed to the ion beam in EATON ion implanter. Ne^{2+} ions were accelerated at 190 kV (resulting in a 380 keV energy) with probe currents of 2.5 μA and a chamber pressure of 5×10^{-7} mbar at room temperature. The chosen fluence is of 2.7×10^{12} ion/cm^2. The projectile trajectory of implanted ions was perpendicular to the surface of the single crystals. The damage profile of V_2AlC single crystal (density of 4.85 g/cm^3) are simulated using the Stopping and Range of Ions in Matter (SRIM) code.[43] The used displacement energies are E_d = 25 eV for V, E_d = 25 eV for Al, and E_d = 28 eV for C.

Chemical exfoliation of V_2AlC single crystal. Ion-implanted V_2AlC single crystals are directly exposed to the chemical etching. With this aim, 20 ml 48% HF (Sigma Aldrich, ≥99.99%) is added in a Teflon vial and placed on the magnetic steering. Ion-implanted single crystals are placed in a plastic vial with small holes in the bottom and partially immersed in the acid solution (*Figure 1c)*. The chemical etching is carried out for 8 h at room temperature under continuous magnetic stirring with the rate of the stir-bar of 500 rpm. After chemical etching the exfoliated crystals are carefully removed from the acid solution and washed multiple times by immersing into deionized water. After washing, the exfoliated crystals were dried and stored inside an argon-filled glovebox.

Structural characterization of V_2AlC single crystal and V_2CT_z MXenes. The X-ray diffraction (XRD) patterns of the V_2AlC single crystals after ion-implantation and chemical etching are collected using a D8 diffractometer (Bruker Ltd. Germany) in Bragg-Brentano geometry, equipped with Cu K_α radiation (1.5406 Å) with a continuous $\theta-2\theta$ scan with 0.017° 2θ/s (U = 40 kV, I = 40 mA). Chemical composition of the chemically etched single crystal was studied using JSM-7001F TTLS field emission gun scanning electron microscope (SEM) (Jeol Ltd., Japan) equipped with an energy dispersive X-ray (EDX) spectrometer from Oxford Instruments (UK). Raman spectroscopy of the single crystals before and after ion-implantation was carried out using a HORIBA Jobin Yvon LabRAM HR800 confocal Raman microscope with a CCD detector. Spectra were acquired at room temperature using an excitation wavelength of 632.8 nm, supplied by an internal He-Ne laser. The power delivered at the sample is 3 mW. An 1800 grooves.mm^{-1} grating is used resulting a spectral resolution of 0.5 cm^{-1}. The spectrometer is calibrated by a silicon wafer. The samples for transmission electron microscopy (TEM) were prepared by lightly scratching the chemically etched surface of ion-implanted V_2AlC single crystals with Cu grid covered with a lacey carbon film so as to deposit MXene flakes on it. The electron energy loss (EEL) spectra were recorded in image mode in a JEOL 2200 FS microscope equipped with an in-column omega filter and operated at 200 kV. The energy resolution determined from the zero-loss peak full width at half-maximum was about 1.0 eV. The core edges (*i.e.*, the C-K, V-$L_{2,3}$ and F-K edges) were extracted from the background signal using a power law and were deconvolved from multiple scattering using the Fourier-ratio method. The EDX analysis were performed using a Bruker XFLASH 6T/60 SDD spectrometer. The topography of the samples was characterized by Atomic Force Microscopy (AFM) in tapping mode using a Dimension 3100 microscope from Bruker.

ASSOCIATED CONTENT

Supporting Information. The Supporting Information is available free of charge on the ACS Publications website. Additional information contains Raman spectra of V_2AlC single crystal before and after Ne^{+2} ion-implantation, chemical composition of V_2AlC single crystal after chemical etching, and F-K edge EEL spectra of exfoliated V_2CT_z flakes.

AUTHOR INFORMATION

Corresponding Authors

*Emails: hanna.pazniak@univ-poitiers.fr (H.P.); marie-laure.david@univ-poitiers.fr (M.-L.D.); vincent.mauchamp@univ-poitiers.fr (V.M.)

Notes

The authors declare no competing financial interest.

ACKNOWLEDGEMENT

This work was supported by the French government program “Investissements d’Avenir” (EUR INTREE, reference ANR-18-EURE-0010). This work was partially funded by the “Région Nouvelle-Aquitaine” and the European Regional Development Fund (ERDF 2014-2021) within the NanoTrans project No. PC-2016-2916910 and by ANR project ANR-18-CE09-0041. The authors thank Marc Marteau for the assistance with ion implantation.

REFERENCES

1. Barsoum, M.W. The $M_{N+1}AX_N$ phases: A New Class of Solids: Thermodynamically Stable Nanolaminates. *Prog. Solid State Chem.* **2000**, *28,* 201-281.

2. Sokol, M.; Natu, V.; Kota, S.; Barsoum, M.W. On the Chemical Diversity of the MAX Phases. *Trends Chem.,* **2019**, *1,* 210-223.

3. Gonzalez-Julian, J. *Processing of MAX phases: From Synthesis to Applications. J Am Ceram Soc.* **2021**, *104,* 659– 690.

4. Naguib, M.; Kurtoglu, M.; Presser, V.; Lu, J.; Niu, J.; Heon, M.; Hultman, L.; Gogotsi, Y.; Barsoum, M.W. Two-Dimensional Nanocrystals Produced by Exfoliation of Ti_3AlC_2. *Adv. Mater.,* **2011**, *23*, 4248-4253.

5. Ajayan, P.; Kim, P.; Banerjee, K. Two-dimensional Van der Waals Materials. *Phys. Today*, **2016**, 69, 38.

6. Barsoum, M. W. MAX Phases: Properties of Machinable Ternary Carbides and Nitrides. Willey, **2013**, 436.

7. Li, Y.; Shao, H.; Lin, Z.; Lu, J.; Liu L.; Duployer, B.; Persson, P. O. Å.; Eklund, P.; Hultman, L.; Li, M.; Chem, K.; Zha, X.-H.; Du, S.; Rozier, P.; Chai, Z.; Raymundo-Pinero, E.; Taberna, P.-L.; Simon, P.; Huang, Q. A General Lewis Acidic Etching Route for Preparing MXenes With Enhanced Electrochemical Performance in Non-Aqueous Electrolyte. *Nat. Mater.* **2020,** *19,* 894–899.

8. EI Ghazaly, A.; Ahmed, H.; Rezk, A.R.; Halim, J. Persson, P. O. Å.; Yeo, L.Y.; Rosen, J. Ultrafast, One-Step, Salt-Solution-Based Acoustic Synthesis of Ti_3C_2 MXene. *ACS Nano*, **2021**, *15*, 4287-4293.

9. Maleski, K.; Mochalin, V.; Gogotsi Y. Dispersion of Two-Dimensional Titanium Carbide MXene in Organic Solvents. *Chem. Mater.* **2017**, *29*, 1632–1640.

10. Carey, M.; Barsoum, M. W. MXene Polymer Nanocomposites: a Review. *Mater. Today Adv,* **2021**, *9*, 100120.

11. Zhang, C.; McKeon, L.; Kremer, M.P.; Park, S.-H.; Ronan, O,; Seral-Ascaso, A.; Barwich, S.; Coileain, C.O.; McEvoy, N.; Nerl, H.C.; Anasori, B.; Coleman, J.N.; Gogotsi, Y.; Nicolosi, V. Additive-Free MXene Inks and Direct Printing of Micro-Supercapacitors. *Nat Commun* **2019**, *10*, 1795.

12. Lipatov, A.; Goad, A.; Loes, M. J.; Vorobeva, N.S.; Abourahma, J.; Gogotsi, Y.; Sinitskii, A. High Electrical Conductivity and Breakdown Current Density of Individual Monolayer $Ti_3C_2T_x$ MXene Flakes, *Matter*, **2021**, *4*, 1413-1427.

13. Lipatov, A.; Alhabeb, M.; Lu, H.; Zhao, S.; Loes, M. J.; Vorobeva, N. S.; Dall'Agnese, Y.; Gao, Y.; Gruverman, A.; Gogotsi, Y.; Sinitskii, A. Electrical and Elastic Properties of Individual Single-Layer $Nb_4C_3T_x$ MXene Flakes. *Adv. Electron. Mater.* **2020**, *6*, 1901382.

14. Pang, J.; Mendes, R.G.; Bachmatiuk, A.; Zhao, L.; Ta, H.A.; Gemming, T.; Liu, H.; Liu, Z.; Rummeli, M.H. Application of 2D MXenes in Energy Conversion and Storage Systems, *Chem. Soc. Rev.* **2019**, *48*, 72-133.

15. Pei, Y.; Zhang, X.; Hui, Z.; Zhou, J.; Huang, X.; Sun, G.; Huang, W. $Ti_3C_2T_x$ MXene for Sensing Application: Recent Progress, Design Principles, and Future Perspectives. *ACS Nano* **2021**, *15*, 3996–4017.

16. Iqbal, A., Sambyal, P.; Koo, C. M. 2D MXenes for Electromagnetic Shielding: A Review. *Adv. Funct. Mater.* **2020**, 30, 2000883.

17. Champagne, A.; Charlier, J.-C. Physical Properties of 2D MXenes: From a Theoretical Perspective. *J. Phys. Mater.* **2021**, *3*, 032006.

18. Khazaei, M.; Ranjbar, A.; Arai, M.; Sasaki, T.; Yunoki, S. Electronic Properties and Application of MXenes: a Theoretical Review. *J. Mater. Chem. C* **2017**, *5*, 2488-2503.

19. Iqbal, A.; Hong, J.; Ko, T.Y.; Koo, C.M. Improving Oxidation Stability of 2D MXenes: Synthesis, Storage Media, and Conditions. *Nano Converg.* **2021**, *8,* 9.

20. Matthews, K.; Zhang, T.; Shuck, C.E.; VahidMohammadi, A.; Gogotsi, Y. Guidelines for Synthesis and Processing of Chemically Stable Two-Dimensional V_2CT_x MXene. *Chem. Mater.* **2022**, *34*, 499–509.

21. Alhabeb, M.; Maleski, K.; Anasori, B.; Lelykh, P.; Clark, L.; Sin, S.; Gogotsi, Y. Guidelines for Synthesis and Processing of 2D Titanium Carbide ($Ti_3C_2T_x$). *Chem. Mater.* **2017**, *29*, 7633−7644.

22. Lipatov, A.; Alhabeb, M.; Lukatskaya, M. R.; Boson, A.; Gogotsi, Y.; Sinitskii, A. Effect of Synthesis on Quality, Electronic Properties and Environmental Stability of Individual Monolayer Ti_3C_2 MXene Flakes. *Adv. Electron. Mater.* **2016**, *2*, 1600255.

23. Ying, G., Kota, S.; Dillon, A.D.; Fafarman, A.T.; Barsoum, M.W. Conductive Transparent V_2CT_x (MXene) Films, *FlatChem* **2018**, *3*, 25-30.

24. Shuck, C.E.; Han, M.; Maleski, K.; Hantanasirisakul, K.; Kim, S.J.; Choi, J.; Reil, W.E.B., Gogotsi, Y. Effect of Ti_3AlC_2 MAX Phase on Structure and Properties of Resultant $Ti_3C_2T_x$ MXene. *ACS Appl. Nano Mater.* **2019**, *2*, 3368–3376.

25. Champagne, A.; Shi, L.; Ouisse, T.; Hackens, B.; Charlier, J.-C. Electronic and Vibrational Properties of V_2C-based MXenes: from Experiments to First-Principles Modelling. *Phys. Rev. B* **2018**, *97*, 115439.

26. Kim, Y., Gkountaras, A.; Chaix-Pluchery, O.; Gelard, I.; Coraux, J.; Chapelier, C.; Barsoum, M.W.; Ouisse, T. Elementary processes governing V_2AlC chemical etching in HF. *RSC Adv.* **2020**, *10*, 25266–25274.

27. Wang, D.; Si, J.; Lin, S.; Zhang, R.; Huang, Y.; Yang, J.; Lu, W.; Zhu, X.; Sun, Y. Achieving Macroscopic $V_4C_3T_x$ MXene by Selectively Etching Al from V_4AlC_3 Single Crystals. *Inorg. Chem.* **2020**, *59*, 3239–3248.

28. Bugnet, M.; Mauchamp, V.; Per Eklund; Jaouen, M.; Cabioch, T. Contribution of Core-Loss Fine Structures to the Characterization of Ion Irradiation Damages in the Nanolaminated Ceramic Ti_3AlC_2. *Acta Mater.*, **2013**, *61*, 7348.

29. Benchakar, M.; Loupias, L.; Garnero, C.; Bilyk, T.; Morais, C.; Canaff, C.; Guignard, N.; Morisset, S.; Pazniak, H.; Hurand, S.; Chartier, P.; Pacaud, J.; Mauchamp, V.; Barsoum, M.W.; Habrioux, A.; Celerier S. One Max Phase, Different MXenes: a Guideline to Understand the Crucial Role of Etching Conditions on Ti3C2Tx Surface Chemistry, *Appl. Surf. Sci.* **2020**, *530*, 147209.

30. Huang, L.; Ding, L.; Wang, H. MXene-Based Membranes for Separation Applications. *Small Sci.* **2021**, *1*: 2100013.

31. Zada, S.; Dai, W.; Kai, Z.; Lu, H.; Meng, X.; Zhang, Y.; Cheng, Y.; Yan, F.; Fu, P.; Zhang, X.; Dong, H. Algae Extraction Controllable Delamination of Vanadium Carbide Nanosheets with Enhanced Near-Infrared Photothermal Performance. *Angew. Chem. Int. Ed.* **2020**, *59*, 6601.

32. Vahidmohammadi, A.; Hadjikhani, A.; Shahbazmohamadi, S.; Beidaghi, M. Two-Dimensional Vanadium Carbide (MXene) as a High-Capacity Cathode Material for Rechargeable Aluminum Batteries. *ACS Nano* **2017**, *11*, 11135−11144.

33. Wang, C.; Yang, T.; Xiao, J.; Liu, S.; Xue, J.; Huang, Q.; Zhang, J.; Wang, J.; Wang, Y. Structural Transitions Induced by Ion Irradiation in V_2AlC and Cr_2AlC. *J. Am. Ceram. Soc.* **2016**, *99*, 1769-1777.

34. Srivastava, P.; Mishra, A.; Mizuseki, H.; Lee, K.-R.; Singh, A.K. Mechanistic Insight into the Chemical Exfoliation and Functionalization of Ti_3C_2 MXene. *ACS Appl. Mater. Interfaces* **2016**, *8*, 24256-64.

35. Surwade, S.P.; Li, Z.; Liu, H. Thermal Oxidation and Unwrinkling of Chemical Vapor Deposition-Grown Graphene, *J. Phys. Chem. C* **2012**, *116*, 38.

36. Seydoux-Guillaume A.M.; Wirth R.; Deutsch A.; Schärer U. Microstructure of 24 – 1928 Ma Concordant Monazites: Implications for Geochronology and Nuclear Waste Deposits. *Geoch. Cosmochim. Acta* **2004**, *68*, 2517-2527.

37. Tunes, M.A.; Harrison, R.W., Donnelly, S.E., Edmondson, F.E. A Transmission Electron Microscopy Study of the Neutron-Irradiation Response of Ti-based MAX phases at High Temperatures. *Acta Materialia* **2019**, *169*, 237-247.

38. David, M.-L.; Beaufort, M.-F., Barbot, J.-F. Effect of Implant Temperature on Defects Created Using High Fluence of Helium in Silicon. *J. Appl. Phys.* **2003**, *93*, 1438-1442.

39. Shi, L.; Ouisse, T.; Sarigiannidou, E.; Chaix-Pluchery, O.; Roussel, H.; Chaussende, D.; Hackens B. Synthesis of Single Crystals of V_2AlC Phase by High-Temperature Solution Growth and Slow Cooling Technique. *Acta Mater.* **2015**, *83*, 304-309.

40. Bylik, T.; Benchakar, M.; Bugnet, M.; Loupias, L.; Chartier, P.; Pazniak, H.; David, M.-L.; Habrioux, A.; Celerier, S.; Pacaud, J.; Mauchamp, V. Electronic Structure Sensitivity to Surface Disorder and Nanometer-Scale Impurity of 2D Titanium Carbide MXene Sheets as Revealed by Electron Energy-Loss Spectroscopy. *J. Phys. Chem. C* **2020**, *124*, 27071–27081.

41. Pazniak, H.; Benchakar, M.; Bylik, T.; Liedl, A.; Busby,Y.; Noël, C.; Chartier, P.; Hurand, S.; Marteau, M.; Houssiau, L.; Larciprete, R.; Lacovig, P.; Lizzit, D.; Tosi, E.; Lizzit, S.; Pacaud, J.; Celerier, S.; Mauchamp, V.; David, M.-L. Ion Implantation as an Approach for Structural Modification and Functionalization of $Ti_3C_2T_x$ MXenes, *ACS Nano* **2021**, *15*, 4245–4255.

42. Magne, D.; Mauchamp, V.; Celerier, S.; Chartier, P.; Cabioch, T. Spectroscopic Evidence in the Visible-Ultraviolet Energy Range of Surface Functionalization Sites in the Multilayer Ti_3C_2 MXene, *Phys. Rev. B* **2015**, *91*, 201409.

43. Ziegler, J.F.; Ziegler, M.D.; Biersack, J.P. SRIM - The Stopping and Range of Ions in Matter. Nucl. Instrum. *Methods Phys. Res., Sect. B* **2010**, *268*, 1818−1823.